

Automated segmentation and extraction of posterior eye segment using OCT scans

Bilal Hassan^{1,†}, Taimur Hassan^{2,†,*}, Ramsha Ahmed³, Shiyin Qin^{1,4}, and Naoufel Werghi²

¹School of Automation Science and Electrical Engineering, Beihang University (BUAA), Beijing 100191, China

²C2PS and KUCARS Centers in Khalifa University of Science & Technology, Abu Dhabi 127788, United Arab Emirates

³School of Computer and Communication Engineering, University of Science & Technology Beijing, Beijing 100083, China

⁴School of Electrical Engineering and Intelligentization, Dongguan University of Technology, Dongguan 523808, China

Abstract—This paper proposes an automated method for the segmentation and extraction of the posterior segment of the human eye, including the vitreous, retina, choroid, and sclera compartments, using multi-vendor optical coherence tomography (OCT) scans. The proposed method works in two phases. First extracts the retinal pigment epithelium (RPE) layer by applying the adaptive thresholding technique to identify the retina-choroid junction. Then, it exploits the structure tensor guided approach to extract the inner limiting membrane (ILM) and the choroidal stroma (CS) layers, locating the vitreous-retina and choroid-sclera junctions in the candidate OCT scan. Furthermore, these three junction boundaries are utilized to conduct posterior eye compartmentalization effectively for both healthy and disease eye OCT scans. The proposed framework is evaluated over 1000 OCT scans, where it obtained the mean intersection over union (IoU) and mean Dice similarity coefficient (DSC) scores of 0.874 and 0.930, respectively.

Index Terms—Posterior Eye Segment, Optical Coherence Tomography (OCT), Segmentation, Extraction, Retina, Choroid.

I. INTRODUCTION

Medical image analysis has been an essential tool in large number of organs pathology including lung [1]–[4], heart [5], colon [6]–[9], cervix [10], eye [11]–[17], and prostate [18], [19]. The eye, in particular, has been the subject of intensive research in medical imaging, especially with visual impairment being leading cause of disability, accounting for over 1 billion confirmed cases worldwide [20]–[24]. Out of many ocular disorders leading to the growing burden of vision loss, most disorders such as diabetic retinopathy, macular edema, and age-related macular degeneration are related to the posterior segment of the human eye [25]–[34]. As the name indicates, the posterior segment is the back part, covering the two-thirds region of the eye. It includes four compartments: vitreous, retina, choroid, and sclera [35]. Optical coherence tomography (OCT) is regarded as one of the most rapidly

emerging imaging methods that allows adequate visualization of both anterior and posterior human eye segment [35]–[45]. However, the number of OCT scans acquired daily has surpassed the capacity of eye specialists in carefully examining these scans, necessitating automated methods to imitate the work of retinal experts [46].

In the past, many researchers have proposed automated algorithms to perform retinal image analysis using OCT scans. These works include detection and segmentation of chorioretinal features [47], [48], classification and grading of retinal diseases [49]–[51], and retinal thickness measurement [52]. However, to the best of our knowledge, very limited research has been conducted on the segmentation and extraction of posterior eye segment. One such work, inspired by the U-Net architecture, is proposed in [35]. While deep learning methods can achieve high accuracy they require larger data cohorts and extensive training time [53]–[63]. Besides, the authors in [35] validated the feasibility of the work considering healthy eyes only. In contrast, this paper proposes an automated method built upon the standard image analysis techniques yet achieving comparable results for both healthy and disease eye OCT scans. The major contributions of this paper are as follows:

- An efficient method for segmenting and extracting the posterior eye compartments (vitreous, retina, choroid, and sclera) for healthy and diseased eye cases using multi-vendor OCT scans.
- An extensive evaluation using 1000 OCT scans, achieving state-of-the-art segmentation results with 0.874 mean intersection over union (IoU) and 0.930 mean Dice similarity coefficient (DSC) scores.

Based on the demonstrated segmentation and extraction results in this paper, the proposed framework can be of great value to upcoming OCT-based studies—for example, estimating retinal fluid in anti-vascular endothelial growth factor (anti-VEGF) therapy and measurement of retina and choroid thickness.

II. PROPOSED METHODOLOGY

The raw OCT scans are pre-processed to convert them to grayscale and resize them to a common resolution of 360×480 before input to the subsequent phases. The high-

This work is supported by a research fund from Khalifa University. Ref: CIRA-2019-047 and the Abu Dhabi Department of Education and Knowledge (ADEK), Ref: AARE19-156. [†]Co-first Authors, ^{*}Corresponding Author, Email: taimur.hassan@ku.ac.ae

© 2021 IEEE. Personal use of this material is permitted. Permission from IEEE must be obtained for all other uses, in any current or future media, including reprinting/republishing this material for advertising or promotional purposes, creating new collective works, for resale or redistribution to servers or lists, or reuse of any copyrighted component of this work in other works.

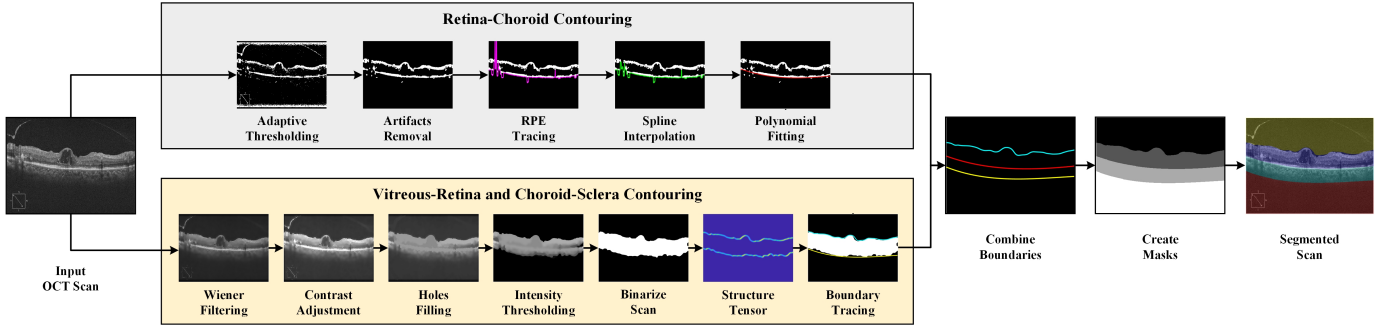


Fig. 1. Proposed framework for segmentation of posterior eye segment.

level overview of the proposed method is demonstrated in Fig. 1, which consists of two main phases as described below:

A. Retina-Choroid Contouring Phase

We extract the RPE layer in this phase, which defines the retina-choroid junction in the candidate OCT scan. Since the RPE layer appears as a hyperreflective element in the OCT scan, the pre-processed input OCT scan is binarized using adaptive thresholding with ‘bright’ foreground polarity. It extracts the brighter contents from the candidate OCT scan, including the RPE layer, ILM layer, along with the unwanted speckle noise artifacts. These unwanted artifacts are removed from the scan using erosion and area opening operations in the next step. Next, to trace the RPE layer junction, a column-wise iterative approach is adopted to locate every last bright point in the OCT scan. Further, the zeros and ‘not a number’ values in the traced RPE layer vector are identified and removed using spline interpolation, as shown in Fig. 1. In the final step, the smoothing operation is carried out using third-order polynomial fitting to obtain the retina-choroid junction.

B. Vitreous-Retina and Choroid-Sclera Contouring Phase

We extract the ILM and CS layers in this phase, defined as the respective vitreous-retina and choroid-sclera junctions in the candidate OCT scan. For this purpose, first, the pre-processed input OCT scan is denoised using Wiener filtering to suppress the speckle noise. Let I be the pre-processed scan containing $N \times M$ sized local neighborhood (η) kernel for each pixel. Then Wiener filter estimates the local mean (μ) and variance (σ^2) around each pixel as expressed in Eq. (1-3):

$$F(n_1, n_2) = \mu + \frac{\sigma^2 + v^2}{\sigma^2} (I(n_1, n_2) - \mu), \quad (1)$$

$$\mu = \frac{1}{NM} \sum_{n_1, n_2 \in \eta} I(n_1, n_2), \quad (2)$$

$$\sigma^2 = \frac{1}{NM} \sum_{n_1, n_2 \in \eta} I^2(n_1, n_2) - \mu^2, \quad (3)$$

where F is the filtered scan and v^2 is the noise variance. Afterward, contrast adjustment is performed to enhance the chorioretinal region intensities followed by hole filling operation. Next, we perform intensity-wise thresholding where more weights are assigned to higher intensity values in

the OCT scan to suppress the background and enhance the chorioretinal region, as shown in Fig. 1. Then, it is binarized to apply the structure tensor (S_T) operation to determine the highly coherent tensor [64]. S_T denotes the second-order moment matrix, which reflects image gradients with prevailing orientation using Gaussian derivative kernels within the given pixel neighborhood, as defined in Eq. (4):

$$S_T = \begin{bmatrix} \omega * (\Delta P \cdot \Delta P) & \omega * (\Delta P \cdot \Delta Q) \\ \omega * (\Delta Q \cdot \Delta P) & \omega * (\Delta Q \cdot \Delta Q) \end{bmatrix}, \quad (4)$$

where ω denotes the Gaussian smoothing filter, and ΔP and ΔQ represent the orientation of image gradients at zero and 90 degrees, respectively. Finally, Canny edge detection is applied to the highly coherent tensor to trace the ILM and CS layers in the final step, obtaining the respective vitreous-retina and choroid-sclera junctions.

C. Segmentation of Posterior Eye Segment

In the final phase, all the three boundary junctions (vitreous-retina, retina-choroid, and choroid-sclera, as shown in Fig. 1) are combined and plotted on a zero-valued 360×480 matrix grid. Finally, the posterior eye segment masks are created using different intensity values between each boundary junction to illustrate the segmentation results. Further, these segmentation results are overlaid on the pre-processed input OCT scan, as shown in Fig. 1.

III. RESULTS

A. Dataset Details

In this research, we have used 1000 OCT scans to evaluate the proposed framework. These scans are collected from four publicly accessible datasets (250 scans each). Farsiu et al. [50] curated the first dataset, which contains OCT scans obtained with the BiopTigen device. Gholami et al. [36] arranged the second dataset, which consists of OCT scans imaged with the Cirrus machine. Similarly, Kermany et al. [49] provided the third dataset with Spectralis OCT scans. The final dataset, organized by Mahmudi et al. [37], contains OCT scans of a Topcon device. The four datasets used in this study are named after the imaging devices they represent. Further, each OCT scan is manually labeled to generate the ground truth data. Table I summarizes the dataset details used in this study.

TABLE I
DATASET DETAILS

Datasets	Pathologies (<i>Scans</i>)
Bioptigen [50]	Healthy (50), AMD (200)
Cirrus [36]	Healthy (50), CSR (75), DR (75), MH (50)
Spectralis [49]	Healthy (25), AMD (75), CNV (75), ME (75)
Topcon [37]	Healthy (250)

AMD = Age-related macular degeneration, CSR = Central serous retinopathy, DR = Diabetic retinopathy, MH = Macular hole, CNV = Choroidal neovascularization, ME = Macular edema.

B. Performance Metrics

The performance of the proposed framework is assessed using four evaluation metrics, including accuracy, IoU, DSC, and boundary F1 (BF) scores. These are defined as follows:

$$Accuracy = \frac{TP + TN}{TP + TN + FP + FN}, \quad (5)$$

$$IoU = \frac{TP}{TP + FP + FN}, \quad (6)$$

$$DSC = \frac{2 \times IoU}{1 + IoU}, \quad (7)$$

$$BF = \frac{2 \times TP}{2 \times TP + FP + FN}, \quad (8)$$

where TP , TN , FP , and FN show the true positive, true negative, false positive, and false negative pixels, respectively.

C. Qualitative Assessment

This section presents the qualitative results for the segmentation of the posterior eye segment (vitreous, retina, choroid, sclera) by the proposed framework. In Fig. 2, the segmentation results are showcased using randomly selected OCT scans from all four datasets investigated in this study. Here, we can observe that segmented regions are almost identical to the corresponding ground truth labels. It evidences the efficacy of the proposed method in producing excellent segmentation results regardless of the dataset and imaging devices. Further, it can be observed from Fig. 2(d) that mainly the erroneous segmented pixels are in case of choroid class near the retina (RPE) and sclera (CS) junctions.

Next, we present the extraction results of the posterior eye segment using the segmentation masks generated by the proposed method. The extraction of retina and choroid is crucial from the perspective of their thickness measurement and for better visualization of chorioretinal anomalies by discarding the artifacts in vitreous and sclera. The extraction results using randomly selected OCT scan from each dataset are shown in Fig. 3. Here, we can appreciate the ability of the proposed method to precisely extract the posterior eye segment.

D. Quantitative Assessment

The performance of the proposed method is quantitatively assessed using various metrics. First, we measure the class-wise metrics to determine the proposed framework performance in terms of individual segmentation of compartments, as shown in Table II. Here, it can be observed that the best

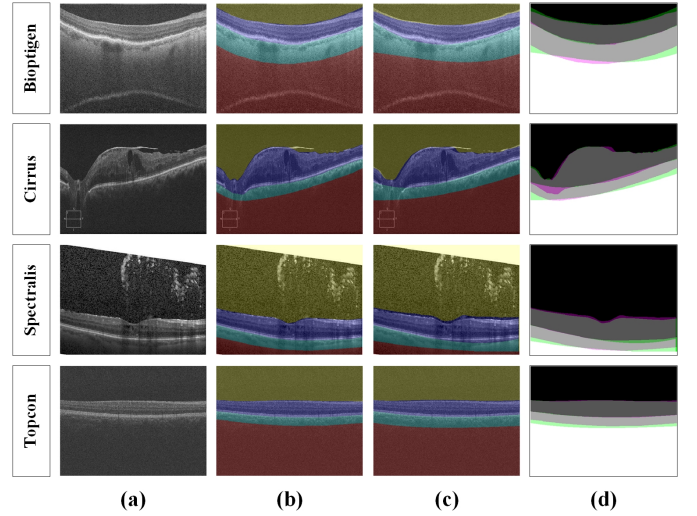


Fig. 2. Segmentation results. (a) Posterior segment OCT scans, (b) Ground truth labels, (c) Segmentation results, (d) Overlapped ground truth and segmented labels. Magenta shows false-positive pixels (over-segmentation), and green depicts the false-negative pixels (under-segmentation).

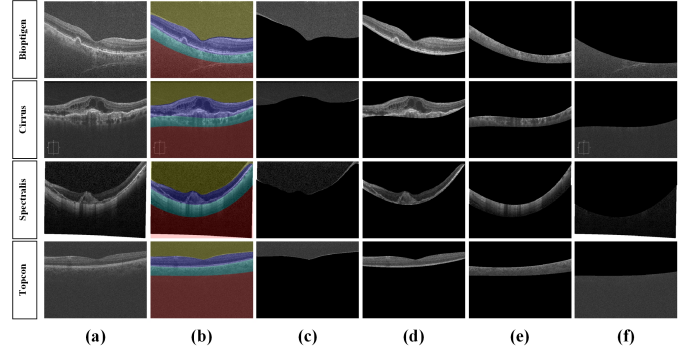


Fig. 3. Extraction results. (a) Posterior segment OCT scans, (b) Segmentation results. Extracted regions using segmentation masks (c) Vitreous, (d) Retina, (e) Choroid, (f) Sclera.

results are achieved for the vitreous class. In contrast, lower performance is observed for the choroid class.

TABLE II
CLASS-WISE METRICS FOR SEGMENTATION OF POSTERIOR EYE SEGMENT.
THE BEST AND THE SECOND-BEST RESULTS ARE SHOWN IN BOLD AND UNDERLINE, RESPECTIVELY.

Metrics	Vitreous	Retina	Choroid	Sclera
IoU	0.969	0.893	0.711	<u>0.921</u>
DSC	0.984	0.944	0.831	<u>0.959</u>
Accuracy	0.987	<u>0.942</u>	0.936	0.925
Mean BF Score	0.902	<u>0.800</u>	0.539	0.701

Next, we present the segmentation performance with respect to datasets and imaging devices, as shown in Table III. We can notice from Table III that the proposed framework achieved the best and second-best performance for the Topcon and Bioptigen OCT scans for all the metrics except weighted IoU, where the second-best value is obtained for Cirrus scans.

On the other hand, it achieved a comparatively low performance for the Cirrus and Spectralis OCT scans. It is perhaps due to fewer variations in terms of retinal conditions (most of the scans belong to the healthy condition) in the Topcon [37] and Bioptigen [50] datasets, making the segmentation task relatively easy for the proposed method. In contrast, the Cirrus [36] and Spectralis [49] datasets are more diversified, complex and contain OCT scans of different retinal pathologies (such as CSR, DR, MH, AMD, CNV, and ME); therefore, in this case, the segmentation of posterior eye segment is a much more complicated task and requires more accuracy.

TABLE III
DATASET-WISE METRICS FOR SEGMENTATION OF POSTERIOR EYE SEGMENT. THE BEST AND THE SECOND-BEST RESULTS ARE SHOWN IN BOLD AND UNDERLINE, RESPECTIVELY.

Metrics	Bioptigen [50]	Cirrus [36]	Spectralis [49]	Topcon [37]	Overall
Global Accuracy	<u>0.946</u>	0.943	0.938	0.968	0.949
Mean Accuracy	<u>0.946</u>	0.943	0.925	0.973	0.948
Mean IoU	<u>0.882</u>	0.856	0.842	0.909	0.874
Weighted IoU	0.902	<u>0.903</u>	0.890	0.943	0.909
Mean BF Score	<u>0.747</u>	0.712	0.665	0.817	0.735

Lastly, we compare the pixel-level results of the proposed framework with the corresponding ground truths using a normalized confusion matrix as shown in Fig. 4. Here, the diagonal row showcases the percentage of correctly segmented pixels for each class. It can be seen from Fig. 4 that the proposed method faced the most confusion (around 8.98%) between the sclera and choroid classes, where 7.48% of the pixels in the sclera class are wrongly segmented as choroid pixels, and 1.50% of the pixels in choroid class are incorrectly segmented as sclera pixels.

True Class	Vitreous	98.75	1.25	0	0
	Retina	3.52	94.18	2.30	0
	Choroid	0.09	4.81	93.61	1.50
	Sclera	0.01	0	7.48	92.51
		Vitreous	Retina	Choroid	Sclera
		Predicted Class			

Fig. 4. Confusion matrix for pixel-level segmentation.

IV. CONCLUSION

This study proposed an automated method to segment the posterior eye compartments, including vitreous, retina, choroid, and sclera. Validated on 1000 scans from four different OCT imaging devices (Bioptigen, Cirrus, Spectralis,

and Topcon), the proposed method demonstrated effective performance in the posterior eye compartmentalization of retinal zones for both healthy and diseased eye candidate scans. Based on the demonstrated segmentation and extraction results, the proposed method adds substantially to the existing retinal image analysis literature. It offers exciting potential in terms of OCT scan compartmentalization for research purposes, observing treatment response, and tracking the disease progression in patients. In the future, this work can be extended to promote the method further to detect various chorioretinal irregularities, providing in-depth analysis of the underlying lesions in terms of detection, segmentation, and objective quantification.

REFERENCES

- [1] F. Taher and other, "Bayesian classification and artificial neural network methods for lung cancer early diagnosis," in *IEEE International Conference on Electronics, Circuits, and Systems*, pp. 773–776, IEEE, 2012.
- [2] F. Taher, N. Werghi, H. Al-Ahmad, and C. Donner, "Extraction and segmentation of sputum cells for lung cancer early diagnosis," *Algorithms*, vol. 6, no. 3, pp. 512–531, 2013.
- [3] M. Sirshar, T. Hassan, M. U. Akram, and S. A. Khan, "An incremental learning approach to automatically recognize pulmonary diseases from the multi-vendor chest radiographs," *Computers in Biology and Medicine*, Vol. 134, 2021.
- [4] T. Hassan, M. U. Akram, M. F. Masood, and U. Yasin, "BIOMISA retinal image database for macular and ocular syndromes," *International Conference Image Analysis and Recognition*, pp. 695–705, 2018.
- [5] S. Ghafoor, A. Nasim, T. Hassan, B. Hassan, and R. Ahmed, "Fully automated identification of heart sounds for the analysis of cardiovascular pathology," *Applications of Intelligent Technologies in Healthcare*, pp. 117–129, 2018.
- [6] A. El Khatib, N. Werghi, and H. Al-Ahmad, "Automatic polyp detection: A comparative study," in *2015 37th Annual International Conference of the IEEE Engineering in Medicine and Biology Society (EMBC)*, pp. 2669–2672, 2015.
- [7] B. Taha, N. Werghi, and J. Dias, "Automatic polyp detection in endoscopy videos: A survey," in *2017 13th IASTED International Conference on Biomedical Engineering (BioMed)*, pp. 233–240, 2017.
- [8] A. Nasim, T. Hassan, M. U. Akram, B. Hassan, and M. A. Shami, "Automated identification of colorectal glands morphology from benign images," *International Conference on Image Processing, Computer Vision, and Pattern Recognition (IPCV)*, pp. 147–152, 2017.
- [9] T. Hassan, B. Hassan, A. El-Baz, and N. Werghi, "A Dilated Residual Hierarchically Fashioned Segmentation Framework for Extracting Gleason Tissues and Grading Prostate Cancer from Whole Slide Images," *IEEE Sensors Applications Symposium (SAS)*, August, 2021.
- [10] B. Taha, J. Dias, and N. Werghi, "Classification of cervical-cancer using pap-smear images: A convolutional neural network approach," in *Medical Image Understanding and Analysis* (M. Valdés Hernández and V. González-Castro, eds.), (Cham), pp. 261–272, Springer International Publishing, 2017.
- [11] T. Hassan, M. U. Akram, B. Hassan, A. Nasim, and S. A. Bazaz, "Review of OCT and fundus images for detection of Macular Edema," *IEEE International Conference on Imaging Systems and Techniques (IST)*, pp. 1–4, 2015.

- [12] M. Asif, S. A. Khan, T. Hassan, M. U. Akram, and A. Shaukat, "Generation of high resolution medical images using super resolution via sparse representation," *International Afro-European Conference for Industrial Advancement*, pp. 288-298, 2016.
- [13] T. Hassan, M. U. Akram, B. Hassan, A. M. Syed, and S. A. Bazaz, "Automated segmentation of subretinal layers for the detection of macular edema," *Applied Optics*, Vol. 55, Issue 3, pp. 454-461, 2016.
- [14] A. M. Syed, T. Hassan, M. U. Akram, S. Naz, and S. Khalid, "Automated diagnosis of macular edema and central serous retinopathy through robust reconstruction of 3D retinal surfaces," *Computer methods and programs in biomedicine*, Vol. 137, pp. 1-10, 2016.
- [15] B. Hassan, G. Raja, T. Hassan, and M. U. Akram, "Structure tensor based automated detection of macular edema and central serous retinopathy using optical coherence tomography images," *Journal of Optical Society of America A*, Vol. 33, Issue 4, pp. 455-463, 2016.
- [16] S. Akbar, T. Hassan, M. U. Akram, U. U. Yasin, and I. Basit, "AVRDB: annotated dataset for vessel segmentation and calculation of arteriovenous ratio," *21th International Conference on Image Processing, Computer Vision, & Pattern Recognition (IPCV)*, pp. 129-134, 2017.
- [17] S. Khalid, M. U. Akram, T. Hassan, A. Nasim, and A. Jameel, "Fully automated robust system to detect retinal edema, central serous chorioretinopathy, and age related macular degeneration from optical coherence tomography images," *BioMed research international*, pp. 217-220, 2017.
- [18] I. Reda, A. Shalaby, F. Khalifa, M. Elmogy, A. Aboulfotouh, M. A. El-Ghar, E. Hosseini-Asl, N. Werghi, R. Keynton, and A. El-Baz, "Computer-aided diagnostic tool for early detection of prostate cancer," in *2016 IEEE International Conference on Image Processing (ICIP)*, pp. 2668-2672, 2016.
- [19] R. Alkadi, D. F. Taher, A. El-Baz, and N. Werghi, "A deep learning-based approach for the detection and localization of prostate cancer in t2 magnetic resonance images," *Journal of Digital Imaging*, vol. 32, 11 2018.
- [20] B. Hassan, R. Ahmed, B. Li, A. Noor, and Z. U. Hassan, "A comprehensive study capturing vision loss burden in Pakistan (1990-2025): Findings from the Global Burden of Disease (GBD) 2017 study," *PloS one*, vol. 14, no. 5, p. e0216492, 2019.
- [21] K. N. Fatima, T. Hassan, M. U. Akram, M. Akhtar, and W. H. Butt, "Fully automated diagnosis of papilledema through robust extraction of vascular patterns and ocular pathology from fundus photographs," *Biomedical optics express*, Vol. 8, Issue 2, pp. 1005-1024, 2017.
- [22] A. W. Arif, A. Nasim, A. M. Syed, and T. Hassan, "Automated diagnosis of retinal edema from optical coherence tomography images," *IEEE International Conference on Computational Science and Computational Intelligence (CSCI)*, pp. 554-557, 2017.
- [23] M. Asif, M. U. Akram, T. Hassan, A. Shaukat, and R. Waqar, "High resolution OCT image generation using super resolution via sparse representation," *Eighth International Conference on Graphic and Image Processing*, Vol. 10225, 2017.
- [24] S. Naz, T. Hassan, M. U. Akram, and S. A. Khan, "A practical approach to OCT based classification of Diabetic Macular Edema," *IEEE International Conference on Signals and Systems (ICSigSys)*, pp. 217-220, 2017.
- [25] B. Hassan, S. Qin, and R. Ahmed, "RRI-Net: Classification of Multi-class Retinal Diseases with Deep Recurrent Residual Inception Network using OCT Scans," in *2020 IEEE International Symposium on Signal Processing and Information Technology (ISSPIT)*, pp. 1-6, IEEE, 2020.
- [26] T. Hassan, A. Usman, M. U. Akram, M. F. Masood, and U. Yasin, "Deep learning based automated extraction of intra-retinal layers for analyzing retinal abnormalities," *IEEE 20th International Conference on e-Health Networking, Applications and Services (Healthcom)*, pp. 1-5, 2018.
- [27] R. Rashid, M. U. Akram, and T. Hassan, "Fully convolutional neural network for lungs segmentation from chest X-rays," *International Conference Image Analysis and Recognition*, pp. 71-80, 2018.
- [28] S. Khalid, M. U. Akram, T. Hassan, A. Jameel, and T. Khalil, "Automated segmentation and quantification of drusen in fundus and optical coherence tomography images for detection of ARMD," *Journal of Digital Imaging*, Vol. 31, Issue 4, pp. 464-476, 2018.
- [29] T. Hassan, M. U. Akram, M. Akhtar, and U. Y. Shoab Ahmad Khan, "Multilayered deep structure tensor delaunay triangulation and morphing based automated diagnosis and 3D presentation of human macula," *Journal of medical systems*, Vol. 42, Issue 11, pp. 1-17, 2018.
- [30] T. Hassan, M. U. Akram, M. F. Masood, and U. Yasin, "Deep structure tensor graph search framework for automated extraction and characterization of retinal layers and fluid pathology in retinal SD-OCT scans," *Computers in biology and medicine*, Vol. 105, pp. 112-124, 2019.
- [31] B. Hassan and T. Hassan, "Fully automated detection, grading and 3D modeling of maculopathy from OCT volumes," *IEEE 2nd International Conference on Communication, Computing and Digital systems (C-CODE)*, pp. 252-257, 2019.
- [32] M. U. Akram, S. Akbar, T. Hassan, S. G. Khawaja, U. Yasin, and I. Basit, "Data on fundus images for vessels segmentation, detection of hypertensive retinopathy, diabetic retinopathy and papilledema," *Data in Brief*, Vol. 29, 2020.
- [33] T. Hassan, M. U. Akram, A. Shaukat, S. G. Khawaja, and B. Hassan, "Structure tensor graph searches based fully automated grading and 3D profiling of maculopathy from retinal OCT images," *IEEE Access*, Vol. 6, pp. 44644-44658, 2018.
- [34] B. Hassan, T. Hassan, B. Li, R. Ahmed, and O. Hassan, "Deep ensemble learning based objective grading of macular edema by extracting clinically significant findings from fused retinal imaging modalities," *Sensors*, Vol. 19, Issue 13, 2019.
- [35] P. M. Maloca, A. Y. Lee, E. R. de Carvalho, M. Okada, K. Fasler, I. Leung, et al., "Validation of automated artificial intelligence segmentation of optical coherence tomography images," *PloS one*, vol. 14, no. 8, p. e0220063, 2019.
- [36] P. Gholami, P. Roy, M. K. Parthasarathy, and V. Lakshminarayanan, "OCTID: Optical coherence tomography image database," *Computers & Electrical Engineering*, vol. 81, p. 106532, 2020.
- [37] T. Mahmudi, R. Kafieh, H. Rabbani, A. M. dehnavi, and M. Akhlagi, "Comparison of macular OCTs in right and left eyes of normal people," in *Medical Imaging 2014: Biomedical Applications in Molecular, Structural, and Functional Imaging*, vol. 9038, pp. 472 - 477, SPIE, 2014.
- [38] T. Hassan, M. U. Akram, and N. Werghi, "Exploiting the Transferability of Deep Learning Systems Across Multi-modal Retinal Scans for Extracting Retinopathy Lesions," *IEEE 20th International Conference on Bioinformatics and Bioengineering (BIBE)*, pp. 577-581, 2020.
- [39] T. Hassan, M. U. Akram, and I. Basit, "Analysis of optical coherence tomography images using deep convolutional neural network for maculopathy grading," *Diabetes and Retinopathy*, pp. 93-108, 2020.
- [40] T. Hassan, M. U. Akram, N. Werghi, and M. N. Nazir, "RAG-FW: A hybrid convolutional framework for the automated extraction of retinal lesions and lesion-influenced grading of human retinal pathology," *IEEE Journal of Biomedical and Health Informatics*, Vol. 25, Issue 1, pp. 108-120, 2020.

- [41] B. Hassan, R. Ahmed, T. Hassan, and N. Werghi, "SIP-SegNet: A deep convolutional encoder-decoder network for joint semantic segmentation and extraction of sclera, iris and pupil based on periocular region suppression," *arXiv:2003.00825*, 2020.
- [42] H. Raja, T. Hassan, M. U. Akram, and N. Werghi, "Clinically verified hybrid deep learning system for retinal ganglion cells aware grading of glaucomatous progression," *IEEE Transactions on Biomedical Engineering*, 2020.
- [43] B. Hassan, S. Qin, T. Hassan, M. U. Akram, R. Ahmed, and N. Werghi, "CDC-Net: Cascaded decoupled convolutional network for lesion-assisted detection and grading of retinopathy using optical coherence tomography (OCT) scans," *Biomedical Signal Processing and Control*, Vol. 70, August, 2021.
- [44] B. Hassan, R. Ahmed, B. Li, O. Hassan, and T. Hassan, "Autonomous Framework for Person Identification by Analyzing Vocal Sounds and Speech Patterns," *IEEE 5th International Conference on Control, Automation and Robotics (ICCAR)*, pp. 325-330, 2019.
- [45] B. Hassan, S. Qin, R. Ahmed, T. Hassan, A. H. Taguri, S. Hashmi, and N. Werghi, "Deep learning based joint segmentation and characterization of multi-class retinal fluid lesions on OCT scans for clinical use in anti-VEGF therapy," *Computers in Biology and Medicine*, August, 2021.
- [46] B. Hassan, S. Qin, and R. Ahmed, "SEADNet: Deep learning driven segmentation and extraction of macular fluids in 3D retinal OCT scans," in *2020 IEEE International Symposium on Signal Processing and Information Technology (ISSPIT)*, pp. 1-6, IEEE, 2020.
- [47] B. Hassan, S. Qin, T. Hassan, R. Ahmed, and N. Werghi, "Joint Segmentation and Quantification of Chorioretinal Biomarkers in Optical Coherence Tomography Scans: A Deep Learning Approach," *IEEE Transactions on Instrumentation and Measurement*, pp. 1-1, 2021.
- [48] B. Hassan, R. Ahmed, and B. Li, "Automated foveal detection in OCT scans," in *2018 IEEE International Symposium on Signal Processing and Information Technology (ISSPIT)*, pp. 419-422, IEEE, 2018.
- [49] D. S. Kermany, M. Goldbaum, W. Cai, C. C. Valentim, H. Liang, S. L. Baxter, *et al.*, "Identifying medical diagnoses and treatable diseases by image-based deep learning," *Cell*, vol. 172, no. 5, pp. 1122-1131, 2018.
- [50] S. Farsiu, S. J. Chiu, R. V. O'Connell, F. A. Folgar, E. Yuan, J. A. Izatt, *et al.*, "Quantitative Classification of Eyes with and without Intermediate Age-related Macular Degeneration Using Optical Coherence Tomography," *Ophthalmology*, vol. 121, no. 1, pp. 162 - 172, 2014.
- [51] B. Hassan and T. Hassan, "Fully automated detection, grading and 3D modeling of maculopathy from OCT volumes," in *2019 2nd International Conference on Communication, Computing and Digital systems (C-CODE)*, pp. 252-257, IEEE, 2019.
- [52] A. Cazañas-Gordón, E. Parra-Mora, and L. A. D. S. Cruz, "Ensemble Learning Approach to Retinal Thickness Assessment in Optical Coherence Tomography," *IEEE Access*, 2021.
- [53] T. Hassan, S. Aslam, and J. W. Jang, "Fully automated multi-resolution channels and multithreaded spectrum allocation protocol for IoT based sensor nets," *IEEE Access*, Vol. 6, pp. 22545-22556, 2018.
- [54] T. Hassan, M. Bettayeb, S. Akçay, S. Khan, M. Bennamoun, and N. Werghi, "Detecting Prohibited Items in X-ray Images: A Contour Proposal Learning Approach," *IEEE International Conference on Image Processing (ICIP)*, pp. 2016-2020, 2020.
- [55] T. Hassan, S. Ahmad, and M. S. Hameed, "Template Matching Based Automated Detection of Curves from Scanned Raster Log Images," *78th EAGE Conference and Exhibition, Issue 1*, pp. 1-5, 2016.
- [56] T. Hassan, S. Akçay, M. Bennamoun, S. Khan, and N. Werghi, "Cascaded structure tensor framework for robust identification of heavily occluded baggage items from X-ray scans," *arXiv*, 2020.
- [57] M. Shafay, T. Hassan, D. Velayudhan, E. Damiani, and N. Werghi, "Deep Fusion Driven Semantic Segmentation for the Automatic Recognition of Concealed Contraband Items," *SoCPar*, pp. 550-559, 2020.
- [58] H. Ahmad, S. M. T. Gillani, T. Omer, T. Hassan, S. Aslam, and S. U. Ali, "Futuristic Short Range Optical Communication: A Survey," *IEEE International Conference on Information Science and Communication Technology (ICISCT)*, 2020.
- [59] T. Hassan, S. Akçay, M. Bennamoun, S. Khan, and N. Werghi, "Unsupervised Anomaly Instance Segmentation for Baggage Threat Recognition," *Journal of Ambient Intelligence and Humanized Computing*, July, 2021.
- [60] M. Shafay, T. Hassan, E. Damiani, and N. Werghi, "Temporal Fusion Based Multi-scale Semantic Segmentation for Detecting Concealed Baggage Threats," *IEEE International Conference on Systems, Man, and Cybernetics (SMC)*, August, 2021.
- [61] T. Hassan and N. Werghi, "Trainable Structure Tensors for Autonomous Baggage Threat Detection Under Extreme Occlusion," *Asian Conference on Computer Vision (ACCV)*, 2020.
- [62] T. Hassan, M. Shafay, S. Akçay, S. Khan, M. Bennamoun, E. Damiani, and N. Werghi, "Meta-Transfer Learning Driven Tensor-Shot Detector for the Autonomous Localization and Recognition of Concealed Baggage Threats," *Sensors*, 2020.
- [63] T. Hassan, S. Akçay, M. Bennamoun, S. Khan, and N. Werghi, "Tensor Pooling Driven Instance Segmentation Framework for Baggage Threat Recognition," *Neural Computing and Applications*, 2021.
- [64] B. Hassan, R. Ahmed, B. Li, O. Hassan, and T. Hassan, "Automated retinal edema detection from fundus and optical coherence tomography scans," in *2019 5th International Conference on Control, Automation and Robotics (ICCAR)*, pp. 325-330, IEEE, 2019.